Mirror modes: Nonmaxwellian distributions

M. Gedalin and Yu. E. Lyubarsky
Ben-Gurion University, Beer-Sheva 84105, Israel

M. Balikhin
ACSE, University of Sheffield, Mappin Street, Sheffield S1 3JD, United Kingdom

C.T. Russell
IGPP/UCLA, 405 Hilgard Ave., Los Angeles, CA 90095-1567

Direct analysis of mirror mode instabilities from the general dielectric tensor for several model distributions, in the long wavelength limit is performed. The growth rate at the instability threshold depends on the derivative of the distribution for zero parallel energy. The maximum growth rate is $\sim k_\parallel v_{T\parallel}$ well above the instability threshold. The instability threshold and growth rate and their dependence on the propagation angle depend on the shapes of the ion and electron distribution functions.

I. INTRODUCTION

Numerous observations of waves in the the Earth magnetosheath, as well as at other planets have stimulated studies of long wavelength and low-frequency modes in high β magnetized plasmas. It has been theoretically shown that the features of low-frequency waves in hot plasmas differ significantly from those in cool plasmas, even in the limit corresponding to the usual magnetohydrodynamic waves [1]. These findings have been subsequently proven by direct comparison with observations [2]. However, particular interest to the low-frequency modes in hot plasmas is explained by observations of the mirror modes, which were found in planetary magnetosheaths [3–8], in the solar wind [9], in cometary comas [10, 11], and in the wake of Io [12, 13]. These modes are nonpropagating zero frequency modes (sometimes considered as the kinetic counterpart of the hydrodynamical entropy mode), which are expected to grow in an anisotropic plasma with sufficiently high $\beta_\perp/\beta_\parallel$ (see, e.g., Hasegawa [14]). Here $\perp$ and $\parallel$ refer to the magnetic field direction, and $\beta_{\perp,\parallel} = 8\pi p_{\perp,\parallel}/B^2$.

The usually observed high amplitudes of mirror modes show that they easily achieve the nonlinear regime. At the same time, in several cases low-amplitude magnetic field structures with the same properties were observed which may mean that the linear and nonlinear mirror mode features are generically related. Yet we do not know so far what makes these modes so ubiquitous and what determines their nonlinear amplitudes.

The early explanation of the mirror instability [14] is based on the simple picture of the adiabatic response of the anisotropic pressure of magnetized particles. Numerical analyses of the mirror instability in bi-Maxwellian plasmas [15–17] (the bi-Maxwellian distribution function is $f(v_\perp, v_\parallel) = (2\pi)^{-3/2}[v_{T\perp}^2 v_{T\parallel}]^{-1}\exp(-v_\perp^2/2v_{T\perp}^2 - v_\parallel^2/2v_{T\parallel}^2)$, where $\perp$ and $\parallel$ refer to the external magnetic field direction) have shown that the maximum of the growth rate occurs at $k_\perp\rho_i \sim 1$ (where ρ_i is the ion thermal gyroradius), which was interpreted as an indication on the kinetic nature of the instability.

At the same time, Southwood and Kivelson [18] proposed a new explanation of the instability mechanism as a resonant one, where the presence of a group of the resonant particles (with $v_\parallel = 0$) plays a *destructive* role in the mode excitation: the growth rate of the instability is claimed to be inversely proportional to the number of the resonant particles. This explanation was further reiterated with some modifications by Pantellini and Schwartz [19] and Pokhotelov et al. [20], and used by Kivelson and Southwood [21] for the explanation of the nonlinear saturation mechanism. The analysis of Southwood and Kivelson [18] is done in the regime where the phase velocity of the perturbation is much less than the parallel thermal velocity, in other words, $\gamma \ll k_\parallel v_{Ti\parallel}$, and therefore, is directly applied only near the threshold of the instability. Well above the threshold the maximum growth rate occurs [17] in the range $\gamma \sim k_\parallel v_{Ti\parallel}$, which is not covered in the previous analytical studies.

The previous analytical and numerical considerations of the linear regime of the mirror instability, even in the long wavelength limit, are, as a rule, restricted to the usage of the bi-Maxwellian distribution. At the same time particle distributions in a collisionless plasma may substantially differ from a Maxwellian. For example, due to the ion heating mechanism at the shock (see, e.g., Sckopke et al. [22]), the magnetosheath ion distributions may well deviate from a bi-Maxwellian. It is therefore of interest to study the dependence of the instability on the shape of the ion and electron distributions.

Yet another argument in favor of the analysis of other distributions is that there is no good analytical approximations for the dielectric tensor for a Maxwellian plasma in the range $|\omega|/k_\parallel v_{T\parallel} \sim 1$, so that one usually has to consider more convenient asymptotics (like $|\omega|/k_\parallel v_{T\parallel} \ll 1$) and further qualitatively extrapolate the results onto the range of interest. It is possible to find shapes for the distribution that allow closed analytical presentation of the dielectric tensor in the whole range of phase velocities and make the study of the instability physics more transparent.

In the present paper we study in detail the dependence of the mirror instability on the shape of the ion and electron distributions, using model distribution functions that allow direct explicit analytical calculation of the dielectric tensor. We establish the generic

relation of the mirror instability with the oscillatory modes when the Landau damping is absent and study the transition to the unstable regime when such damping exists. We also propose an approximation that is useful for the analytical treatment of the instability well above the threshold where $\gamma \sim k_\parallel v_{Ti\parallel}$. The analysis is carried out in the long wavelength limit. From numerical analyses it is known that the absolute maximum of the growth rate is achieved when $k_\parallel v_{T\parallel} \lesssim k_\perp v_{T\perp} \lesssim \Omega$ [17] so that a short wavelength analysis is needed for comparison with observations. Such analysis does not seem possible (analytically) at present. However, the long wavelength consideration allows to understand the basic physics of the instability and qualitatively extrapolate the results onto the short wavelength range.

The paper is organized as follows. In section II we derive the general dispersion relation in the long wavelength approximation for an arbitrary distribution function. In sections III-IV we apply the general analysis to three different distributions. In section V we derive the instability condition and the growth rate at the threshold for an arbitrary distribution. In section VI we develop a useful approximation for the analysis of the bi-Maxwellian-like distributions in the region of maximum growth rate.

II. DISPERSION RELATION IN THE LONG WAVELENGTH LIMIT

In what follows we will be interested in the long wavelength limit where $\omega \ll \Omega$ and $kv_T \ll \Omega$ (where $\Omega = eB/mc$ is the gyrofrequency and v_T is the thermal velocity), while maintaining a finite phase velocity $0 < \omega/k < \infty$. The last inequality means that the phase velocity does not tend to zero over the entire range of propagation angles but it certainly may vanish for a particular set of parameters. For simplicity we assume that both ions and electrons are Maxwellian in the perpendicular direction, so that $\langle v_\perp^2 \rangle = 2v_{T\perp}^2$ and $\langle v_\perp^4 \rangle = 8v_{T\perp}^4$. We also denote $\langle v_\parallel^2 \rangle = v_{T\parallel}^2$ and $\beta_{\parallel,\perp} = 2v_{T\parallel,\perp}^2\omega_p^2/c^2\Omega^2$ for each species (subscript i stands for ions and subscript e for electrons, $\omega_p = \sqrt{4\pi q_s^2 n_s/m_s}$ is the plasma frequency for species s). Here $\langle F \rangle = \int F f v_\perp dv_\perp dv_\parallel$ denotes averaging over the distribution function which is assumed to be separable $f = f_\perp(v_\perp) f_\parallel(v_\parallel)$ and normalized so that $\langle 1 \rangle = 1$. Let us introduce the refraction index vector $\mathbf{N} = \mathbf{k}c/\omega$, such that $\mathbf{N} = (N_\perp, 0, N_\parallel) = N(\sin\theta, 0, \cos\theta)$. With all this the components of the dispersion matrix $D_{ij} = N^2\delta_{ij} - N_i N_j - \epsilon_{ij}$ take the following form (see Appendices A and B):

$$D_{11} = N_\parallel^2 \left(1 - \tfrac{1}{2}(\beta_\parallel - \beta_\perp)\right) - 1 - \frac{\omega_{pi}^2}{\Omega_i^2} - \frac{\omega_{pe}^2}{\Omega_e^2}, \tag{1}$$

$$D_{12} = 0, \tag{2}$$

$$D_{13} = -N_\parallel N_\perp \left(1 - \tfrac{1}{2}(\beta_\parallel - \beta_\perp)\right), \tag{3}$$

$$D_{22} = N^2 \left[1 - \tfrac{1}{2}\cos^2\theta(\beta_\parallel - \beta_\perp) + \sin^2\theta\beta_\perp \right. \tag{4}$$
$$\left. - \sin^2\theta(r_i\beta_{i\perp}\bar{\chi}_i + r_e\beta_{e\perp}\bar{\chi}_e)\right] - 1 - \frac{\omega_{pi}^2}{\Omega_i^2} - \frac{\omega_{pe}^2}{\Omega_e^2},$$

$$D_{23} = -i\frac{\omega_{pi}^2 \tan\theta}{\Omega_i\omega}\left(r_i\bar{\chi}_i - r_e\bar{\chi}_e\right), \tag{5}$$

$$D_{33} = N_\perp^2 \left(1 - \tfrac{1}{2}(\beta_\parallel - \beta_\perp)\right) - 1 - \frac{\omega_{pi}^2\beta_{i\parallel}}{k_\parallel^2 v_{Ti\parallel}^2}\left(\frac{\bar{\chi}_i}{\beta_{i\parallel}} + \frac{\bar{\chi}_e}{\beta_{e\parallel}}\right) \tag{6}$$
$$+ \frac{\omega_{pi}^2\tan^2\theta}{\Omega_i^2} r_i\bar{\chi}_i + \frac{\omega_{pe}^2\tan^2\theta}{\Omega_e^2} r_e\bar{\chi}_e,$$

where $\beta_\parallel = \beta_{i\parallel} + \beta_{e\parallel}$, $\beta_\perp = \beta_{i\perp} + \beta_{e\perp}$, $r_i = \beta_{i\perp}/\beta_{i\parallel}$, $r_e = \beta_{e\perp}/\beta_{e\parallel}$, and

$$\bar{\chi} = v_{T\parallel}^2 \int (\omega/k_\parallel - v_\parallel)^{-1} \frac{\partial f}{\partial v_\parallel} dv_\parallel. \tag{7}$$

The integration in (7) is taken along the path below the singularity $v_\parallel = \omega/k_\parallel$. In what follows we shall also assume that $\omega_{pi}^2/\Omega_i^2 \gg 1$ and neglect unity relative to this large parameter (which corresponds to the assumption $v_A \ll c$, where $v_A = c\Omega_i/\omega_{pi}$ is the Alfven velocity). In what follows we also neglect $\omega_{pe}^2/\Omega_e^2 = (\omega_{pi}^2/\Omega_i^2)(m_e/m_i)$. In the above derivation we used $\omega_{pi}^2/\Omega_i = -\omega_{pe}^2/\Omega_e$ in the quasineutral electron proton plasma (this is not correct if any admixture of other charged particles is present).

In the limit $\omega/\Omega_i \to 0$ (and ω/k finite) the dispersion relation $D = \det\|D_{ij}\| = 0$ splits into two. One describes the purely transverse Alfven wave (the wave electric field vector in the $\mathbf{kB}_0$ plane, the wave magnetic field vector perpendicular to the external magnetic field) with the dispersion

$$\omega^2 = k^2 v_A^2 \cos^2\theta \left(1 - \tfrac{1}{2}(\beta_\parallel - \beta_\perp)\right). \tag{8}$$

In this wave the absolute value of the magnetic field does not change, but the magnetic field rotates.

The second dispersion relation is

$$\Psi(Z) = \left[2 - \cos^2\theta(\beta_\parallel - \beta_\perp) + 2\sin^2\theta\beta_\perp - 2\sin^2\theta(r_i\beta_{i\perp}\bar{\chi}_i + r_e\beta_{e\perp}\bar{\chi}_e)\right.$$
$$\left. -Z^2\beta_{i\parallel}\cos^2\theta\right]\left[\frac{\bar{\chi}_i}{\beta_{i\parallel}} + \frac{\bar{\chi}_e}{\beta_{e\parallel}}\right] + \sin^2\theta\left[r_i\bar{\chi}_i - r_e\bar{\chi}_e\right]^2 = 0, \tag{9}$$

where we introduce $Z = \omega/k_\parallel v_{Ti\parallel}$ for convenience (ω is complex, in general, so that $Z = W + iG$), and $r_{i,e} = \beta_{i,e\perp}/\beta_{i,e\parallel}$. Eq. (9) describes elliptically polarized waves with all three components of the wave electric field present, so that in general there exists a nonzero component of the wave magnetic field $B_z = N_\perp E_y$ in the direction of the external magnetic field. These waves not only rotate the magnetic field but change its magnitude as well.

The functions $\bar{\chi}$ play a crucial role in the subsequent analysis. They are defined by the integral containing the distribution function $f(v_\parallel)$ and cannot be explicitly calculated without a particular choice of these distributions. It is common to choose f as Maxwellian. In this case $\bar{\chi}$ is well-known and tabulated but has good asymptotic expansions only for $|Z| \ll 1$ or $|Z| \gg 1$ (for electrons $Z\sqrt{m_e/m_i}(v_{Ti\parallel}/v_{Te\parallel})$ should be substituted for Z). This restricts possible analytical considerations of the mirror instability to the range $|Z| \ll 1$. Yet, numerical analyses [15] show that when the system is well above the instability threshold, the maximum growth rate is achieved in the vicinity of $|Z| \sim 1$, which is unavailable to direct theoretical analysis when a Maxwellian is chosen. On the other hand, there are indications that the qualitative features of long waves (instabilities) in the high β plasma more or less sensibly depend on the lowest moments of the distribution function (provided it is sufficiently "normal": smooth, no beams, no holes, etc.). It therefore makes sense to investigate the dispersion relations for a suitably chosen model distribution so that $\bar{\chi}$ can be calculated and analyzed in the range $|Z| \sim 1$. In what follows we shall use three different distributions for these purposes. The waterbag distribution $f = \Theta(v_0^2 - v_\parallel^2)/2v_0$ will be used for study of the behavior of long wavelength modes and their dependence on the plasma parameters in the absence of Landau damping. Here $\Theta(x) = 1$ if $x > 0$ and $\Theta(x) = 0$ if $x < 0$. The hard-bell distribution $f = 3(v_0^2 - v_\parallel^2)\Theta(v_0^2 - v_\parallel^2)/4v_0^3$ will allow to include the Landau damping effects, and the Lorentz-like distribution $f = (2v_0^3/\pi)(v_0^2 + v_\parallel^2)^{-2}$ removes the upper limit on the particle velocities. The four distributions (including Maxwellian $f = (2\pi v_{T\parallel}^2)^{-1/2}\exp(-v_\parallel^2/2v_{T\parallel}^2)$) mentioned in this paper are shown in Figure 1.

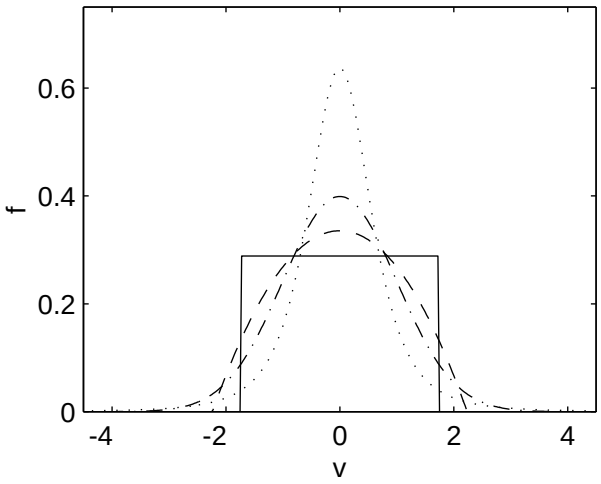

FIG. 1: Waterbag (solid line), hard bell (dashed), Lorentzian (dotted), and Maxwellian (dash-dotted) distributions.

III. WATERBAG DISTRIBUTION

The waterbag distribution $f = \Theta(v_0^2 - v_\parallel^2)/2v_0$ is somewhat peculiar since the Landau damping is absent. The analysis of this distribution allows the establishing of the generic relation of the instability to nondamping propagating modes. It is easy to show that in this case

$$\bar{\chi}_i = \frac{1}{3 - Z^2}, \qquad \bar{\chi}_e = \frac{1}{3 - Z^2\mu R} \tag{10}$$

where $\mu = m_e/m_i \approx 1/2000$, $R = \beta_{i\|}/\beta_{e\|}$, and $v_{T\|}^2 = v_0^2/3$. In the limit $Z = 0$ one has $d \equiv \bar{\chi}(Z = 0) = 1/3$. It is worth noting that for the Maxwellian distribution $d = 1$. In this section for electrons we use the approximation of the massless bi-Maxwellian (instead of the above waterbag,which is used only for ions), for which $\bar{\chi}_e = 1$. The resulting dispersion relation (9) is a third order equation with respect to Z^2 with real coefficients. Although this equation can be analyzed directly and even solved analytically, graphical representation of the roots is much more convenient. The onset of the instability can be analyzed in a quite general way (see section V).

Figure 2 shows the mode with the highest phase velocity (fast mode) for the case when $\beta_{i\|} = \beta_{i\perp} = \beta_{e\|} = \beta_{e\perp} = 0.1$

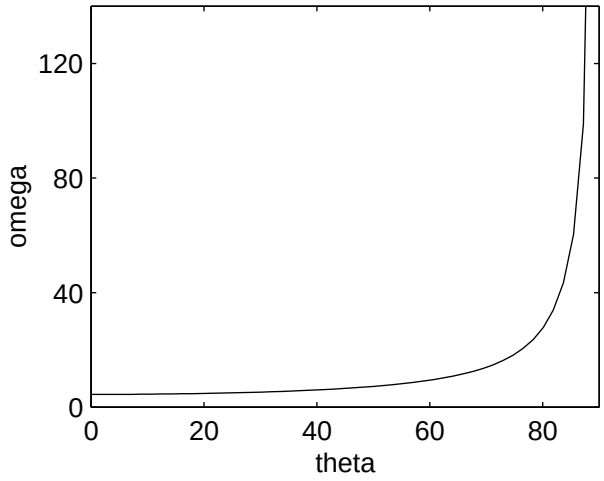

FIG. 2: Phase velocity of the fast mode as a function of propagation angle for the case of the waterbag distribution with $\beta_{i\|} = \beta_{i\perp} = \beta_{e\|} = \beta_{e\perp} = 0.1$ and massless bi-Maxwellian electrons.

and with massless bi-Maxwellian electrons. It it worth noting that ions are *not* isotropic since they are Maxwellian in the perpendicular direction and waterbag in the parallel direction. The phase velocity of the fast mode is well above $v_{Ti\|}$ so that it does not participate in the mirror instability. We do not consider this mode in the rest of the paper. We do not consider the Alfven mode either. The remaining two low-phase velocity modes are shown in Figure 3 together with $\omega = k_\| v_{0i}$ (solid line).

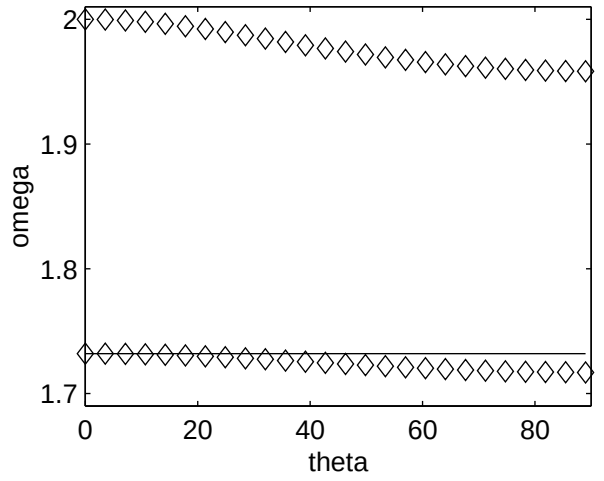

FIG. 3: Phase velocity (diamonds) of the two low-velocity modes as a function of propagation angle for the case of the waterbag distribution with $\beta_{i\|} = \beta_{i\perp} = \beta_{e\|} = \beta_{e\perp} = 0.1$ and massless bi-Maxwellian electrons. The solid line is $\omega = \sqrt{a_i} k_\| v_{Ti\|} = k_\| v_{0i}$.

For the upper curve the resonance $v_\| = \omega/k_\|$ is impossible. This is the waterbag analog of the slow mode. The lower mode is inside the resonant region and would damp if there were a nonzero $\partial f/\partial v_\|$. Figure 2 and all subsequent figures are plotted for $\omega \ll \Omega$ and $kv_T \ll \Omega$.

Figure 4 shows the same two modes but in the case $\beta_{i\|} = \beta_{i\perp} = \beta_{e\|} = \beta_{e\perp} = 0.5$. There is not much difference in the

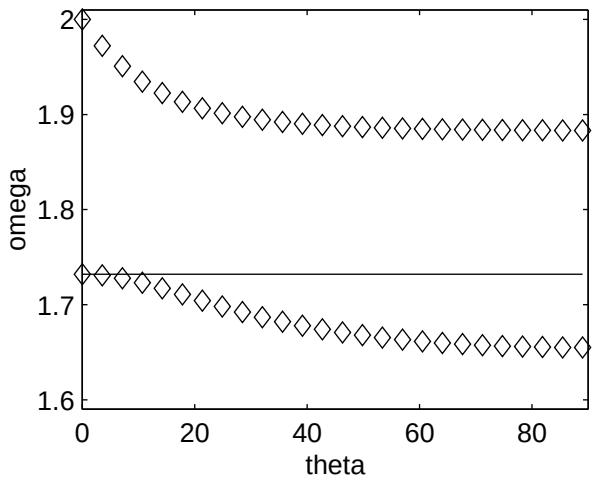

FIG. 4: Phase velocity (diamonds) of the two low-velocity modes as a function of propagation angle for the case of the waterbag distribution with $\beta_{i\parallel} = \beta_{i\perp} = \beta_{e\parallel} = \beta_{e\perp} = 0.5$ and massless bi-Maxwellian electrons. The solid line is $\omega = \sqrt{a_i} k_\parallel v_{Ti\parallel} = k_\parallel v_{0i}$.

behavior of the two modes for these two cases, except a little stronger decrease of the phase velocities towards the perpendicular propagation regime in the higher $\beta_\perp$ case.

Figure 5 shows the behavior of the two modes in the anisotropic case $\beta_{i\parallel} = \beta_{e\parallel} = 0.1$, $\beta_{i\perp} = \beta_{e\perp} = 0.5$, and bi-Maxwellian

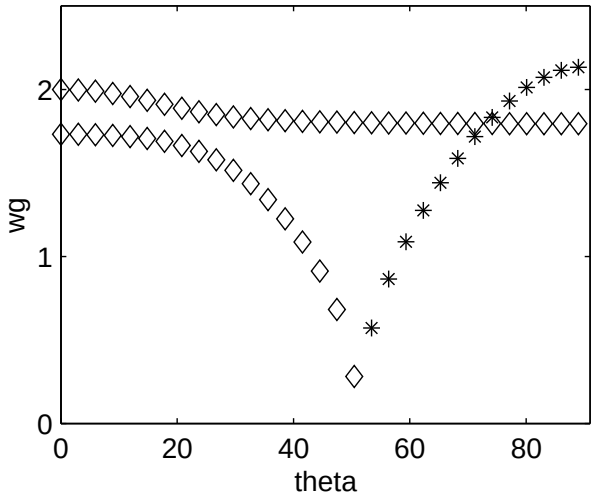

FIG. 5: Behavior of the two low-velocity modes as a function of propagation angle for the case of the waterbag distribution with $\beta_{i\parallel} = \beta_{e\parallel} = 0.1$, $\beta_{i\perp} = \beta_{e\perp} = 0.5$, and massless bi-Maxwellian electrons. Diamonds mark the modes in the range where their frequencies are purely real, stars show the growth rate of the aperiodic instability.

electrons. The lower mode now remains purely propagating mode for smaller angles (diamonds) but turns into an aperiodic instability for larger angles of propagation (stars). The obvious conclusion from Figure 5 is that the unstable mode has its propagation counterpart for the smaller angles of propagation. The relative growth rate $G = \gamma/k_\parallel v_{Ti\parallel} \sim 1$ is large in the whole range of instability, so that the approximation $G \ll 1$ [18] is not applicable.

It is of interest to compare this case with the massless waterbag electrons $\bar{\chi}_e = 1/3$. The corresponding curves in Figure 6 show that there is no instability in this case. Thus, the analysis of the waterbag distribution shows that (a) there is, in general, a propagating counterpart of the mirror instability if Landau damping is absent, (b) the instability threshold and growth rate are sensitive to the details of the distribution and not only to the second moment (see the explanation in section V), and (c) the instability is aperiodic, that is, in the unstable range $W = 0$ and $G > 0$. It can be shown that the last feature is generally valid unless the distribution function is very peculiar (see Appendix C).

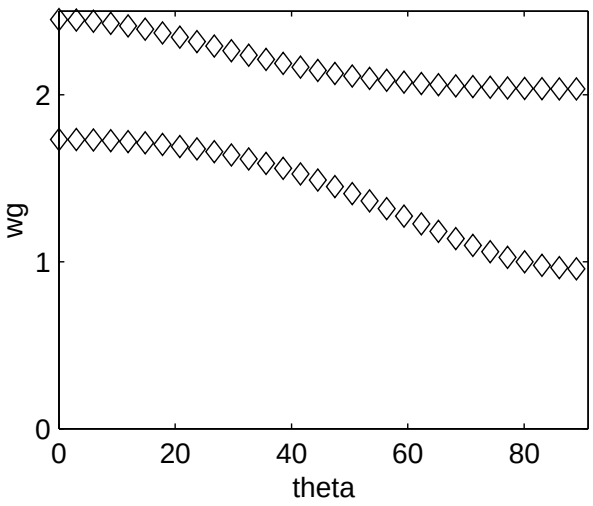

FIG. 6: Behavior of the two low-velocity modes as a function of propagation angle for the case of the waterbag distribution with $\beta_{i\parallel} = \beta_{e\parallel} = 0.1$, $\beta_{i\perp} = \beta_{e\perp} = 0.5$, and waterbag electrons, $d_e = 1/3$. There is no instability.

IV. HARD-BELL AND LORENTZIAN DISTRIBUTIONS

The waterbag distribution does not allow Landau damping since $\partial f/\partial v_\parallel = 0$ everywhere. In order to get rid of this restriction we consider the hard-bell distribution $f = 3(v_0^2 - v_\parallel^2)\Theta(v_0^2 - v_\parallel^2)/4v_0^3$, which has nonzero derivative but is is compact ($f = 0$ for $|v_\parallel| > v_0$). In this case

$$\bar{\chi}_i = \frac{3}{5}\left[1 + \frac{Z}{4\sqrt{5}}\ln\frac{(\sqrt{5}-W)^2+G^2}{(\sqrt{5}+W)^2+G^2} + \frac{iZ}{2\sqrt{5}}\left(\arctan\frac{\sqrt{5}-W}{G} + \arctan\frac{\sqrt{5}+W}{G}\right)\right], \tag{11}$$

where $Z = W + iG$, W and G being real, $G > 0$, and $v_0^2 = 5v_{T\parallel}^2$. The corresponding $d = \bar{\chi}(Z = 0) = 3/5$. The corresponding expression for $\bar{\chi}_e$ is obtained from (11) by substitution $Z \to Z\sqrt{\mu R}$.

In order to analyze non-compact distributions too we shall consider the Lorentzian distribution $f = (2v_0^3/\pi)(v_0^2 + v_\parallel^2)^{-2}$. In this case

$$\bar{\chi}_i = \frac{16iZ}{(1+Z^2)^3} + \frac{3i}{i-Z} - \frac{2Z}{(i-Z)^3} + \frac{3iZ}{(i-Z)^2}, \tag{12}$$

with $v_0^2 = v_{T\parallel}^2$ and $d = 3$. Again, $\bar{\chi}_e$ is obtained by substitution $Z \to Z\sqrt{\mu R}$.

We shall also compare the results for these distributions with the bi-Maxwellian. In this case there is no compact analytical expression for χ and we use direct numerical calculation.

In what follows we are interested only in the unstable region. The "subparticle" mode is expected to be strongly damped in the propagation range. The "superparticle" mode is not damped in the hard-bell case and almost not damped in the Lorentzian case.

As the first set of parameters for the unstable regime we choose $\beta_{i\parallel} = \beta_{e\parallel} = 0.1$, $\beta_{i\perp} = \beta_{e\perp} = 0.5$, and massless bi-Maxwellian electrons $\bar{\chi}_e = 1$. Figure 7 shows the growth rates for the three distributions. The highest growth rate is for the Lorentzian, the lowest is for the waterbag. Figure 8 shows the same growth rates as in Figure 7 but normalized by $kv_{Ti\parallel}$ which allows to compare growth rates of the modes with the same wavenumber k and different angles of propagation. It is seen that the maximum growth rates is achieved approximately at $\theta \approx 50 - 60^\circ$ for all distributions, moving sllightly towards smalles angles for Maxwellian and Lorentzian. The threshold angle moves substantially towards more quasiparallel regimes for distributions with stronger tails (Maxwellian and Lorentzian).

Figure 9 shows the dependence of the growth rate on $\beta_\perp$ for the same anisotropy ratio and when $\beta_{i\perp}/\beta_{e\perp} = \beta_{i\parallel}/\beta_{e\parallel} = 1$ remain constant. Both curves correspond to the waterbag ions and massless bi-Maxwellian electrons. Diamonds stand for the same parameters as in Figure 5, crosses correspond to $\beta_{i\perp} = 1$ and $\beta_{i\parallel} = 0.2$. The instability is stronger for higher $\beta_\perp$.

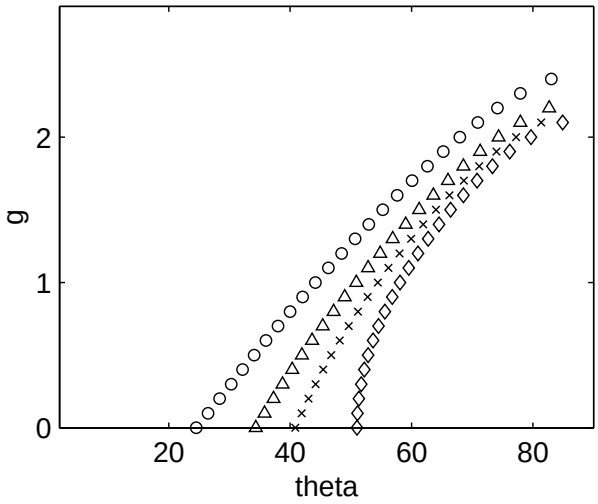

FIG. 7: Growth rates for the mirror instability in the case of $\beta_{i\|} = \beta_{e\|} = 0.1$, $\beta_{i\perp} = \beta_{e\perp} = 0.5$, and massless bi-Maxwellian electrons $d_e = 1$, and four different distributions: waterbag (diamonds), hard-bell (crosses), Lorentzian (circles), and bi-Maxwellian (triangles).

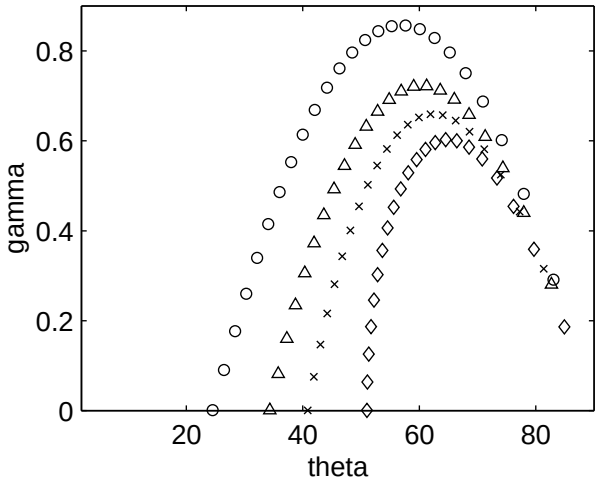

FIG. 8: Growth rates for the mirror instability in the case of $\beta_{i\|} = \beta_{e\|} = 0.1$, $\beta_{i\perp} = \beta_{e\perp} = 0.5$, and massless bi-Maxwellian electrons $d_e = 1$, and four different distributions: waterbag (diamonds), hard-bell (crosses), Lorentzian (circles), and bi-Maxwellian (triangles), normalized by $kv_{Ti\|}$.

In the previous analysis we always used the approximation of massless bi-Maxwellian distribution corresponding to $\chi_e = 1$. Figures 10 and 11 show the growth rate of the instability when the electron distributions are chosen in the same form as the ion distributions. The waterbag distributions become stable, while the growth rate in the case of Lorentzian drastically increases. The ratio of the maximum growth rates shown in Figures 8 and 11 roughly corresponds to $d_e = \chi_e(Z = 0)$ which shows that the maximum growth rate depends significantly on electrons (see sections V and VI).

For other combinations of ion and electron distributions the ratios may be even greater as is seen in Figure 12, where diamonds correspond to waterbag ions and massless bi-Maxwellian electrons, while circles correspond to waterbag ions and Lorentzian electrons. The β parameters are the same for both cases.

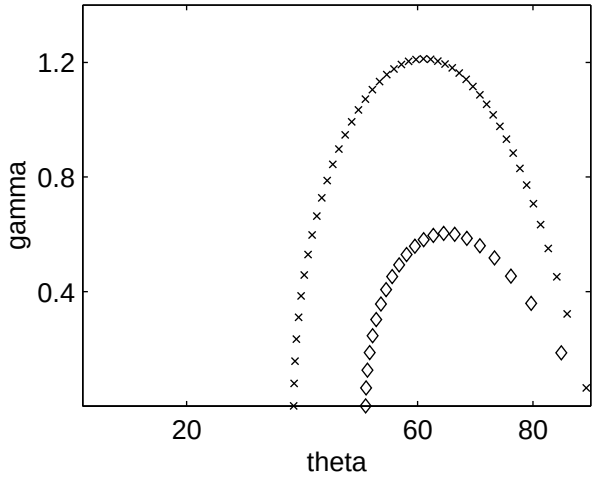

FIG. 9: Dependence of the growth rate on $\beta_\perp$ for waterbag ions and massless bi-Maxwellian electrons: diamonds correspond to $\beta_{i\parallel} = \beta_{e\parallel} = 0.1$, $\beta_{i\perp} = \beta_{e\perp} = 0.5$, crosses correspond to $\beta_{i\parallel} = \beta_{e\parallel} = 0.2$, $\beta_{i\perp} = \beta_{e\perp} = 1$.

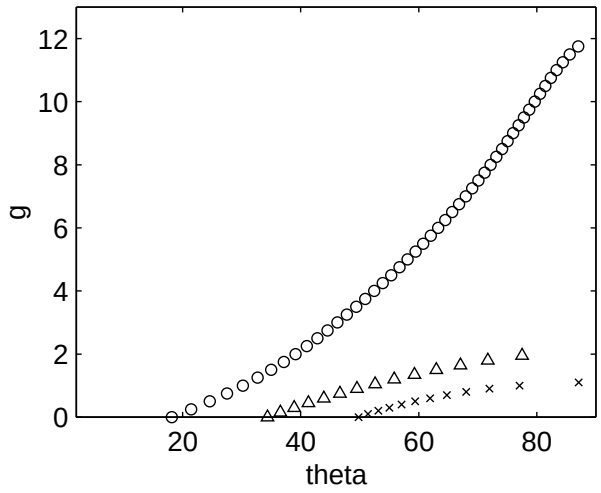

FIG. 10: Growth rates for the mirror instability in the case of $\beta_{i\parallel} = \beta_{e\parallel} = 0.1$, $\beta_{i\perp} = \beta_{e\perp} = 0.5$, and three different combinations: hard-bell ions and electrons (crosses), Lorentzian ions and electrons (circles), and bi-Maxwellian ions and (massive) electrons (triangles).

V. NEAR THE THRESHOLD

It is possible to obtain general results just above the threshold of the instability, where $Z = iG \to +0$. For $f = f(v^2)$ it is easy to show

$$\begin{aligned}\chi &= \int \frac{1}{iG - v_\parallel} \frac{\partial f}{\partial v_\parallel} dv_\parallel \\ &= -\int \frac{v_\parallel}{v_\parallel^2 + G^2} \frac{\partial f}{\partial v_\parallel} dv_\parallel = -\int \frac{df}{d\mathcal{E}} dv_\parallel + G \int \frac{G}{v_\parallel^2 + G^2} \frac{df}{d\mathcal{E}} dv_\parallel \\ &= -\int \frac{df}{d\mathcal{E}} dv_\parallel + \pi G \frac{df}{d\mathcal{E}}|_{v_\parallel = 0} = d - \kappa G,\end{aligned} \tag{13}$$

where $\mathcal{E} = v_\parallel^2/2$ is the energy (per unit mass). Substituting this into (9) and neglecting all terms of the order Z^2 and higher, one has

$$G = -A/B, \tag{14}$$

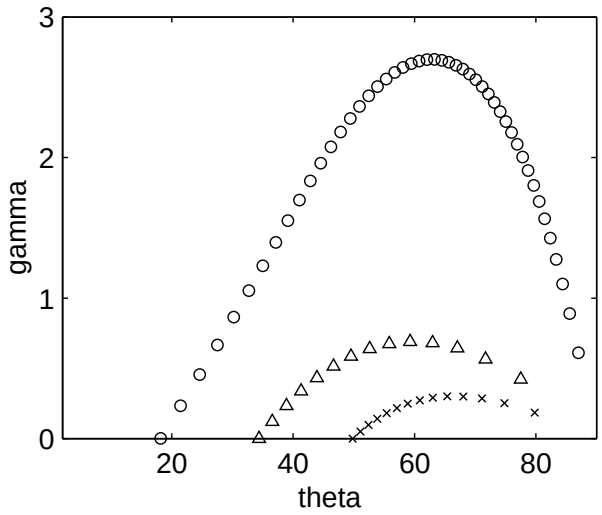

FIG. 11: Same as in Figure 10 but normalized by $kv_{Ti\|}$.

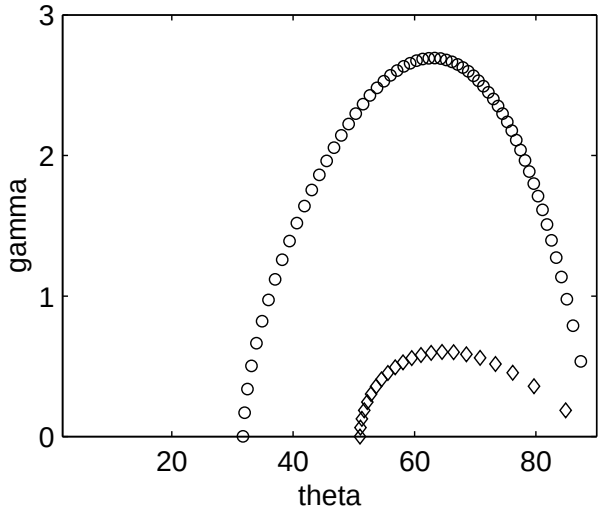

FIG. 12: Growth rates for the mirror instability in the case of $\beta_{i\|} = \beta_{e\|} = 0.1$, $\beta_{i\perp} = \beta_{e\perp} = 0.5$, waterbag ions and two different electron distributions: massless bi-Maxwellian (diamonds) and Lorentzian (circles).

$$A = [2 - \cos^2\theta(\beta_\| - \beta_\perp) + 2\sin^2\theta\beta_\perp - 2\sin^2\theta(r_i\beta_{i\perp}d_i + r_e\beta_{e\perp}d_e)]\left(\frac{d_i}{\beta_{i\|}} + \frac{d_e}{\beta_{e\|}}\right) + \sin^2\theta(r_id_i - r_ed_e)^2, \tag{15}$$

$$B = -\frac{\kappa_i}{\beta_{i\|}}[2 - \cos^2\theta(\beta_\| - \beta_\perp) + 2\sin^2\theta\beta_\perp - 2\sin^2\theta(r_i\beta_{i\perp}d_i + r_e\beta_{e\perp}d_e)] + 2\sin^2\theta r_i\beta_{i\perp}\kappa_i\left(\frac{d_i}{\beta_{i\|}} + \frac{d_e}{\beta_{e\|}}\right) - 2\sin^2\theta\kappa_i(r_id_i - r_ed_e), \tag{16}$$

where we neglected $\kappa_e \sim \kappa_i\sqrt{m_e/m_i}$. The instability threshold for a given θ is found from the condition $G = 0$, that is, $A = 0$, which gives

$$2 + \beta_\perp - \beta_\| + \sin^2\theta[\beta_\| + \beta_\perp - 2(r_i\beta_{i\perp}d_i + r_e\beta_{e\perp}d_e) + (r_id_i - r_ed_e)^2/(d_i/\beta_{i\|} + d_e/\beta_{e\|})] = 0. \tag{17}$$

Since $0 \le \sin^2\theta \le 1$, the global instability criterion becomes (in the assumption that $2+\beta_\perp > \beta_\parallel$):

$$2(r_i\beta_{i\perp}d_i + r_e\beta_{e\perp}d_e) - 2 - 2\beta_\perp - (r_id_i - r_ed_e)^2\left(\frac{d_i}{\beta_{i\parallel}} + \frac{d_e}{\beta_{e\parallel}}\right)^{-1} > 0. \tag{18}$$

When $r_e = r_i = \beta_\perp/\beta_\parallel$ and $d_e = d_i = d$, one gets

$$\frac{d\beta_\perp}{\beta_\parallel} > 1 + \frac{1}{\beta_\perp}. \tag{19}$$

This condition is harder for more compact distributions ($d = 1/3$ for waterbag and $d = 3/5$ for hard-bell) and softer for distributions with long tails ($d = 1$ for Maxwellian and $d = 3$ for Lorentzian). The global instability condition (18) can be written in a more symmetric form as follows:

$$\begin{aligned}(r_id_i + r_ed_e)^2 + \frac{2(\beta_{i\perp}^2 + \beta_{e\perp}^2)d_ed_i}{\beta_{i\parallel}\beta_{e\parallel}} \\ - 2(1+\beta_\perp)\left(\frac{d_e}{\beta_{e\parallel}} + \frac{d_i}{\beta_{i\parallel}}\right) > 0\end{aligned} \tag{20}$$

which emphasizes the symmetric role of ions and electrons in the instability onset (cf. Pokhotelov et al. [20]).

Indeed, near the threshold $\gamma/k_\parallel v_{T\parallel} \ll 1$ and the response of both electrons and ions is adiabatic, that is, their inertia does not play any role. In these circumstances the mass of the particle is of not importance. Their role in the response to the parallel electric field is, however, antisymmetric because of the different signs of the charge: the adiabatic response is obtained from $eE_z - (1/n)(dp/dz) = eE_z - ik_\parallel p/n = 0$. The parallel response plays a crucial role in the instability development. As is known the instability occurs because of the breakdown of the local frozen-in condition and efficient drag of particles out of the field enhancement into the field depletion region [18–20]. Thus, when the magnetic field is perturbed, $B_z = B_0 + \delta B_z$, the perturbation of the density of the species s is

$$\frac{\delta n_s}{n_{0s}} = \frac{\delta B_z}{B_0} + \frac{\delta n_s^{(\mathrm{ext})}}{n_{0s}}, \tag{21}$$

where $\delta n_s^{(\mathrm{ext})}$ is due to the motion along the field lines. In the adiabatic regime $\gamma/k_\parallel v_{T\parallel} \ll 1$ this change can be considered as a quasistatic response to the effective potential $\phi_{\mathrm{eff}} = \phi + \mu_s\delta B_z/q_s$, where ϕ is the electrostatic potential, $\mu_s = \langle v_\perp^2\rangle_s/2B_0$ is the average magnetic moment, and q_s is the charge of the species. The density response to this effective potential can be found from the reduced Vlasov equation for the distribution function perturbation δf_s of the species s (f_s is the unperturbed ditribution function)

$$\frac{\partial \delta f_s}{\partial t} + v_\parallel\frac{\partial \delta f_s}{\partial z} = q_s\frac{\partial \phi_{\mathrm{eff}}}{\partial z}\frac{\partial f_s}{\partial v_\parallel}, \tag{22}$$

which for $\partial/\partial t = \gamma$ and $\partial/\partial z = ik_\parallel$ gives

$$\frac{\delta n_s^{(\mathrm{ext})}}{n_{0s}} = q_s\phi_{\mathrm{eff}}\int\frac{ik_\parallel}{\gamma + ik_\parallel v_\parallel}\frac{\partial f_s}{\partial v_\parallel}dv_\parallel. \tag{23}$$

It is easy to see that in the adiabatic regime near the threshold of the instability, $\gamma \to 0$, this expression reduces to the following

$$\frac{\delta n_s^{(\mathrm{ext})}}{n_{0s}} = -\frac{q_s\phi_{\mathrm{eff}}}{4\pi n_{0s}q_s^2r_D^2}, \tag{24}$$

where r_D is the Debye length calculated with the parallel distribution function. It is easy to see that $r_D^2 = v_{T\parallel}^2/\omega_p^2 d$, where $d = \bar{\chi}(Z=0)$. The electrostatic potential ϕ can be excluded using the quasineutrality condition $\delta n_e = \delta n_i$, which eventually gives

$$\frac{\delta n}{n} = \frac{\delta B_z}{B_0}\left[1 - \frac{T_{e\perp} + T_{i\perp}}{4\pi e^2 n_0(r_{De}^2 + r_{Di}^2)}\right], \tag{25}$$

where we have taken into account that $\mu = T_\perp/B_0$. Eq. (25) shows that smaller Debye lengths r_D (larger d) result in the stronger drag of the particles into the weak field region, thus reducing the kinetic pressure response to the magnetic field enhancement

and supporting instability. Therefore, stronger Debye screening (larger d) would lower the instability threshold, in agreement with that found from rigorous calculations. This effect is responsible for the disappearance of the mirror instability in the case of waterbag ions and waterbag electrons considered in section III.

It is worth noting that for bi-Maxwellian distributions Eq. (25) takes the following form:

$$\frac{\delta n}{n} = \frac{\delta B_z}{B_0}\left[1 - \frac{T_{e\perp} + T_{i\perp}}{T_{e\parallel} + T_{i\parallel}}\right], \tag{26}$$

and in the case $T_{e\perp} = T_{e\parallel}$ reproduces the expression found by Pantellini and Schwartz [19].

From (14)–(16) it is easily seen that the growth rate is inversely proportional to $\kappa_i = -\pi(df/d\mathcal{E})|_{v_\parallel=0}$, and not to the number of particles with $v_\parallel = 0$ (cf. Southwood and Kivelson [18]). The latter is correct for the bi-Maxwellian distribution since $(df/d\mathcal{E}) \propto f$ in this case. For other distributions this relation may well be wrong (see also Rose [23] for stability of mirror modes for general distribution functions). For example, for the waterbag distribution $(df/d\mathcal{E})|_{v_\parallel=0} = 0$ and higher order terms should be retained to investigate the behavior near the threshold. It is easy to see from (13) that in this case $\bar\chi = d - \alpha G^2$, where $\alpha = -\int v_\parallel^{-2}(df/d\mathcal{E})dv_\parallel$ is well-defined. The dispersion relation (9) becomes then a first order equation for G^2, which has one positive solution near the threshold. It is clear that in this case the growth rate is determined by the whole distribution and not only by the behavior at $v_\parallel = 0$.

VI. HYDRODYNAMICAL REGIME

The previous analysis shows that maximum Z is of the order of unity or larger (unless the plasma is close to the stability threshold), which means that ions no longer respond adiabatically to the magnetic field enhancements and their inertia begins to play an important role. This also means that it is the thermal particles of the ion distribution body with $v \sim v_{Ti\parallel}$ that are mainly responsible for the instability development and not only the group of resonant particles with $v_\parallel = 0$. Figure 10 shows that for some distributions the instability may be very fast so that the electron inertia should be taken into account.

The previous analysis gives a clue to the treatment of the instability in the range of maximum growth rates, where $G \gtrsim 1$. Let us assume that the distribution function is such that $v_\parallel f(v_\parallel)$ has a sharp maximum at some $v_m \sim v_{T\parallel}$. An example of a distribution of this kind is the Maxwellian $f_i = (1/\sqrt{2\pi}v_{Ti\parallel})\exp(-v_\parallel^2/2v_{Ti\parallel}^2)$ for which there was no good approximation for $\bar\chi$ in the range $|Z| \sim 1$ so far. For the aperiodic mirror instability with $Z = iG$, $G > 0$, one has

$$\bar\chi = \int \frac{1}{iG - v_\parallel}\frac{\partial f}{\partial v_\parallel}dv_\parallel = -\int \frac{1}{G^2 + v_\parallel^2} v_\parallel \frac{\partial f}{\partial v_\parallel}dv_\parallel. \tag{27}$$

The physical sense of this expression is that the dynamical plasma response to the fast growing perturbations [24] should be substituted for the static one (see section V).

For $v_m \sim 1 \lesssim G$ (v_m is normalized on $v_{T\parallel}$) the function $(G^2 + v_\parallel^2)^{-1}$ varies slowly in the vicinity of the maximum of $v_\parallel(\partial f/\partial v_\parallel)$, so that one may approximate

$$\bar\chi = -\frac{1}{G^2 + v_m^2}\int v_\parallel \frac{\partial f}{\partial v_\parallel}dv_\parallel = \frac{1}{G^2 + v_m^2}. \tag{28}$$

Figure 13 shows the comparison of the numerically found $\bar\chi$ for the Maxwellian distribution ($v_m^2 = 2$) and $Z = iG, G > 0$ with the approximation (28). The approximation proves to be very good for $G \geq 1$ and is only a factor 2 smaller at $G \to 0$. Figure 14 shows a similar comparison for a Lorentzian. Now the maximum growth rate can be obtained by substituting $\bar\chi_i = 1/(G^2 + v_{mi}^2)$ in (9). If G is expected to be high, so that $G^2 R\mu \sim 1$, as it occurs for the Lorentzian $e - i$ distributions in Figure 10, the electron inertia should be also taken into account by substituting $\bar\chi_e = 1/(G^2 R\mu + v_{me}^2)$. If, however, the growth rates are relatively modest (as in other cases studied in the present paper), the electrons still respond adiabatically and $\bar\chi_e = d_e$. In the last case (9) turns into a third order equation with respect to G^2. Finding the maximum growth rate from this equation is a technical problem. The physical sense of the above approximation is that it is the paticles with $v_\parallel \sim v_m$ which conribute mainly to the dynamical screening. The higher is v_m the weaker is the screening [24]. As is shown in section V screening plays the destabilizing role, so that we can expect that smaller v_m would correspond to higher growth rates. This can be seen already from Figure 8 where the growth rate for the Lorentzian ions, $v_m^2 = 0.5$, is larger than the growth rate for the Maxwellian, $v_m^2 = 2$ (with the same massless Maxwellian electrons). Figure 15 shows the comparison of the growth rates obtained with the proposed approximation for several $v_m^2 = 2$ (diamonds), 1.5 (crosses), 1 (triangles), 0.5 (circles), and massless Maxwellian electrons. Different v_m model different shapes of the distribution function. The parameters chosen are $\beta_{i\perp} = \beta_{e\perp} = 0.5$, $\beta_{i\parallel} = \beta_{e\parallel} = 0.1$. As expected the decrease of v_m results in the increase of the maximum growth rate.

Finally, Figure 16 shows the comparison of the growth rates obtained directly and with the above approximation for Maxwellian (diamonds and crosses) and Lorentzian (triangles and circles) distributions, for the same parameter set. The agreement is quite satisfactory.

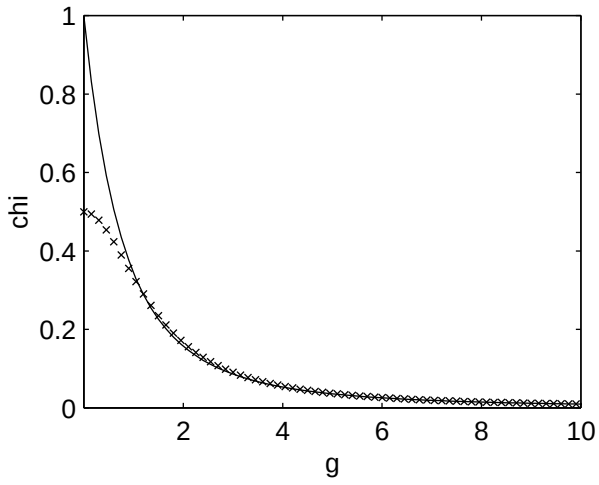

FIG. 13: Approximation of $\chi(G)$ for the Maxwellian distribution. The numerically calculated $\chi(G)$ (solid line) is compared to $\chi = (G^2+2)^{-1}$ (crosses).

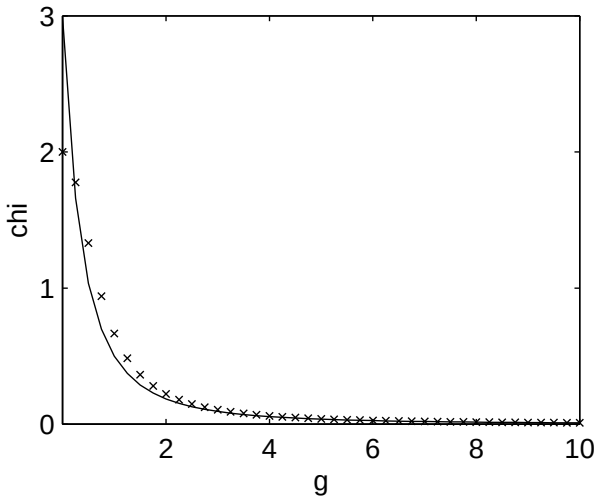

FIG. 14: Approximation of $\chi(G)$ for the Lorentzian distribution. The numerically calculated $\chi(G)$ (solid line) is compared to $\chi = (G^2 + 0.5)^{-1}$ (crosses).

VII. CONCLUSIONS

We have derived the most general dispersion relation for long wavelength modes in hot plasmas. We have derived the general mirror instability condition for arbitrary ion and electron distributions and growth rate of the instability near the threshold. The instability threshold depends not only on the ion and electron β but also on another integral characteristic of the distribution function $d = \int v_\parallel^{-1}(\partial f/\partial v_\parallel)dv_\parallel$ for both species. Larger d corresponds to smaller Debye length. Smaller Debye length, in turn, corresponds to stronger response of the density to the perturbations of the potential, which allows stronger density depletions in the regions of the magnetic field enhancements. Therefore, the kinetic pressure response to the magnetic pressure buildup weakens. Hence, the larger is d the lower is the instability threshold. The near-the-threshold growth rate is inversely proportional to $\partial f/\partial\mathcal{E}$, where $\mathcal{E} = v_\parallel^2/2$ is the parallel energy.

The mirror instability is always aperiodic and $(\gamma/k_\parallel v_{Ti\parallel})_{\max} \sim 1$ (and sometimes substantially greater) for the plasma well above the instability threshold. Maximum growth rates are normally determined by the velocity v_{mi} such that $v_\parallel \partial f_i/\partial v_\parallel$ has a sharp maximum in $v_\parallel = v_{mi}$, and d_e (if the instability is very strong v_{me} takes the place of d_e). This is related to the dynamic redistribution in which the thermal particles participate. Growth rates are higher for distributions with tails and lower for compact distributions (those, for which $f = 0$ if $|v_\parallel| > v_0$, where v_0 is some upper limit). For noncompact distributions the maximum growth rate is larger for smaller v_m, which corresponds to a weaker dynamic screening of the parallel electric

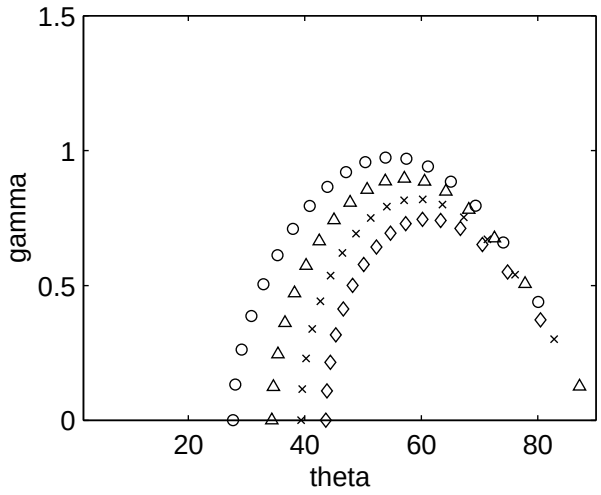

FIG. 15: Growth rates for the mirror instability in the case of $\beta_{i\parallel} = \beta_{e\parallel} = 0.1$, $\beta_{i\perp} = \beta_{e\perp} = 0.5$, calculated with the approximation $\bar{\chi}_i = 1/(G^2 + v_m^2)$, for several $v_m^2 = 2$ (diamonds), 1.5 (crosses), 1 (triangles), and 0.5 (circles). The electrons are massless Maxwellian.

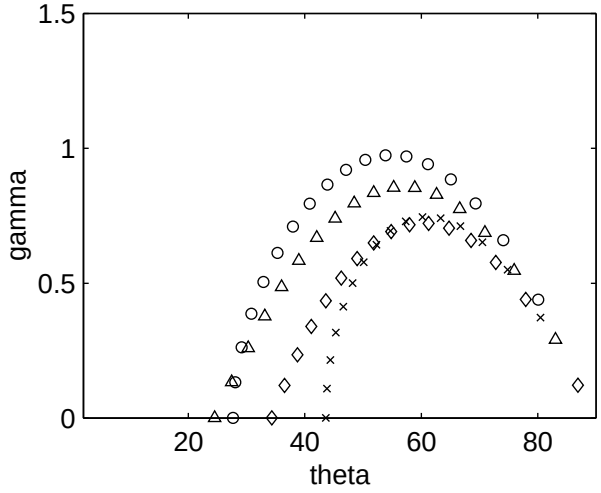

FIG. 16: Comparison of the growth rates for the mirror instability in the case of $\beta_{i\parallel} = \beta_{e\parallel} = 0.1$, $\beta_{i\perp} = \beta_{e\perp} = 0.5$, calculated directly and with the approximation $\bar{\chi}_i = 1/(G^2 + v_m^2)$, for Maxwellian (diamonds and crosses, respectively) and Lorentzian (triangles and circles, respectively). The electrons are massless Maxwellian.

field. For the distributions analyzed in this paper the behavior of d and v_m correlates (d increases when v_m decreases) since all these are single-parameter distributions. For more general distributions the behavior of d_e and v_m may be uncorrelated. It is also worth noting that it is not, in general, any specific group of particles which are responsible for the instability development. Compare, for example, two similar distributions (velocity normalized by the thermal velocity $v_{T\parallel}$): $f_1 = (2/\pi)(1 + v_\parallel^2)^{-2}$ with $d = 3$ and $v_m^2 = 0.5$, and $f_2 = (\sqrt{2}/\pi)(1 + v_\parallel^4)^{-1}$ with $d = 1$ and $v_m^2 = 1$. While the behavior of the two is similar for $v_\parallel = 0$ and $v_\parallel \to \infty$ (the only difference is the factor $\sqrt{2}$), the first one is expected to be more unstable because of the three times stronger Debye screening. At the same time the behavior of the second distribution near the threshold should be close to that of the Maxwellian, $d = 1$, despite the very different suprathermal tails and $(df/d\mathcal{E})|_{v_\parallel=0}$.

We have also proposed a useful approximation for the dielectric function in the range $G/k_\parallel v_{Ti\parallel} \gtrsim 1$ for distributions with sharp maxima of $v_\parallel(\partial f/\partial v_\parallel)$ (a Maxwellian is one such distribution). This approximation proves to be quite satisfactory for Maxwellian type distributions and allows the analytical study of the behavior of the instability in the maximum growth rate range in the long wavelength limit.

Acknowledgments

M. Gedalin and M. Balikhin are grateful to the ISSI for supporting meetings and discussions within the framework of the workshops of the "Waves in the high-β plasma" team. Figures in the paper were prepared using Matlab.

Appendix A: General expressions

We start with the general expression for the dielectric tensor in the following form:

$$\epsilon_{ij} = \delta_{ij} + \sum \lambda_{ij}, \tag{A1}$$

where the summation is on the species and

$$\lambda_{ij} = -\frac{\omega_p^2}{\omega^2}\delta_{ij} + \eta_{ij}. \tag{A2}$$

The expression for η_{ij} is well-known (see, e.g., Hasegawa [14]):

$$\eta_{ij} = -\sum_n \frac{\omega_p^2}{\omega^2}\int v_\perp dv_\perp dv_\parallel \left(\frac{n\Omega}{v_\perp}\frac{\partial f_0}{\partial v_\perp} + k_\parallel \frac{\partial f_0}{\partial v_\parallel}\right)\frac{\Pi_{ij}}{n\Omega - \zeta}, \tag{A3}$$

where $\zeta = \omega - k_\parallel v_\parallel$, and

$$\Pi_{ij} = \begin{pmatrix} (n^2\Omega^2/k_\perp^2)J_n^2 & i(v_\perp n\Omega/k_\perp)J_nJ_n' & (v_\parallel n\Omega/k_\perp)J_n^2 \\ -i(v_\perp n\Omega/k_\perp)J_nJ_n' & v_\perp^2 {J_n'}^2 & -iv_\perp v_\parallel J_nJ_n' \\ (v_\parallel n\Omega/k_\perp)J_n^2 & iv_\perp v_\parallel J_nJ_n' & v_\parallel^2 J_n^2 \end{pmatrix}. \tag{A4}$$

Here $J_n = J_n(x)$, $x = k_\perp\rho = k_\perp v_\perp/\Omega$, and $J_n' = dJ_n/dx$.

For the analysis in the low-frequency range $\omega/\Omega \ll 1$ let us write

$$\eta_{ij} = \eta_{ij}^{(0)} + \eta_{ij}^{(n\neq 0)}, \tag{A5}$$

and expand

$$\frac{1}{n\Omega - \zeta} = \frac{1}{n\Omega}\left(1 + \frac{\zeta}{n\Omega} + \frac{\zeta^2}{n^2\Omega^2} + \cdots\right).$$

Let also $f_0 = f_1(v_\perp)f_2(v_\parallel^2)$, and denote $\langle \ldots \rangle = \int (\ldots) f dv_j$, where $j = \perp, \parallel$.

One has

$$\eta_{ij}^{(0)} = \frac{\omega_p^2}{\omega^2}\int v_\perp dv_\perp dv_\parallel \frac{k_\parallel}{\zeta}\frac{\partial f_0}{\partial v_\parallel} \times \begin{pmatrix} 0 & 0 & 0 \\ 0 & v_\perp^2 {J_0'}^2 & -iv_\perp v_\parallel J_0J_0' \\ 0 & iv_\perp v_\parallel J_0J_0' & v_\parallel^2 J_0^2 \end{pmatrix} \tag{A6}$$

and

$$\begin{aligned} \eta_{ij}^{(n\neq 0)} = &-\sum \frac{\omega_p^2}{\omega^2}\int v_\perp dv_\perp dv_\parallel \left(\frac{1}{v_\perp}\frac{\partial f_0}{\partial v_\perp} + \frac{k_\parallel}{n\Omega}\frac{\partial f_0}{\partial v_\parallel}\right) \\ &\times \left(1 + \frac{\zeta}{n\Omega} + \frac{\zeta^2}{n^2\Omega^2}\right)\Pi_{ij}. \end{aligned} \tag{A7}$$

Now, up to Ω^{-2} one obtains

$$\eta_{11}^{(n\neq 0)} = -\sum_n \frac{\omega_p^2}{\omega^2}\left[\langle J_n^2 \frac{\partial}{\partial v_\perp}\rangle \frac{n^2\Omega^2 + \omega^2 + k_\parallel^2\langle v_\parallel^2\rangle}{k_\perp^2} + \frac{k_\parallel^2}{k_\perp^2}\langle v_\perp J_n^2\rangle\right], \tag{A8}$$

$$\eta_{12}^{(n\neq 0)} = -i\sum_n \frac{\omega_p^2}{\omega^2}\frac{\omega}{k_\perp}\langle v_\perp J_nJ_n'\frac{\partial}{\partial v_\perp}\rangle, \tag{A9}$$

$$\eta_{13}^{(n\neq 0)} = \sum_n \frac{\omega_p^2}{\omega^2}\frac{k_\parallel}{k_\perp}\left[\langle v_\perp J_n^2\rangle + \langle v_\parallel^2\rangle\langle J_n^2\frac{\partial\rangle}{\partial v_\perp}\right], \tag{A10}$$

$$\eta_{22}^{(n\neq 0)} = -\sum_n \frac{\omega_p^2}{\omega^2}\left[\langle v_\perp^2 {J_n'}^2\frac{\partial}{\partial v_\perp}\rangle\left(1+\frac{\omega^2+k_\parallel^2\langle v_\parallel^2\rangle}{n^2\Omega^2}\right)+\frac{k_\parallel^2}{n^2\Omega^2}\langle v_\perp^3 {J_n'}^2\rangle\right], \tag{A11}$$

$$\eta_{23}^{(n\neq 0)} = -i\sum_n \frac{\omega_p^2 k_\parallel}{\omega n^2\Omega^2}\left[\langle v_\perp^2 J_n J_n'\rangle + 2\langle v_\parallel^2\rangle\langle v_\perp J_n J_n'\frac{\partial}{\partial v_\perp}\rangle\right], \tag{A12}$$

$$\eta_{33}^{(n\neq 0)} = -\sum_n \frac{\omega_p^2}{\omega^2}\langle v_\parallel^2\rangle\langle J_n^2\frac{\partial}{\partial v_\perp}\rangle, \tag{A13}$$

and

$$\eta_{22}^{(0)} = \frac{\omega_p^2}{\omega^2}k_\parallel\langle v_\perp^3 {J_0'}^2\rangle\chi, \tag{A14}$$

$$\eta_{23}^{(0)} = -i\frac{\omega_p^2}{\omega}\langle v_\perp^2 J_0 J_0'\rangle\chi, \tag{A15}$$

$$\eta_{33}^{(0)} = \frac{\omega_p^2}{\omega^2}\langle v_\perp J_0^2\rangle\left(1+\frac{\omega^2}{k_\parallel}\chi\right). \tag{A16}$$

where

$$\chi = \langle\frac{1}{\zeta}\frac{\partial}{\partial v_\parallel}\rangle. \tag{A17}$$

Using summation rules [25] one obtains eventually the following general expression for λ_{ij} in the limit of $\omega, k_\parallel v_\parallel \ll \Omega$ when expanded up to the second order in ζ/Ω:

$$\lambda_{11} = \frac{\omega_p^2}{k_\perp^2}\left(1+\frac{k_\parallel^2\langle v_\parallel^2\rangle}{\omega^2}\right)\langle J_0^2\frac{\partial}{\partial v_\perp}\rangle - \frac{\omega_p^2}{\omega^2}\frac{k_\parallel^2}{k_\perp^2}\langle v_\perp(1-J_0^2)\rangle, \tag{A18}$$

$$\lambda_{12} = i\frac{\omega_p^2}{\omega k_\perp}\langle v_\perp J_0 J_0'\frac{\partial}{\partial v_\perp}\rangle, \tag{A19}$$

$$\lambda_{13} = \frac{\omega_p^2}{\omega^2}\frac{k_\parallel}{k_\perp}\left[\langle v_\perp(1-J_0^2)\rangle - \langle v_\parallel^2\rangle\langle J_0^2\frac{\partial}{\partial v_\perp}\rangle\right], \tag{A20}$$

$$\lambda_{22} = \frac{\omega_p^2}{\omega^2}\langle v_\perp^2 {J_0'}^2\frac{\partial}{\partial v_\perp}\rangle - \frac{\omega_p^2}{\omega^2}\sum_n\left[\frac{\omega^2+k_\parallel^2\langle v_\parallel^2\rangle}{n^2\Omega^2}\langle v_\perp^2 {J_n'}^2\frac{\partial}{\partial v_\perp}\rangle\right. \tag{A21}$$

$$\left.+\frac{k_\parallel^2}{n^2\Omega^2}\langle v_\perp^3 {J_n'}^2\rangle\right] + \frac{\omega_p^2}{\omega^2}k_\parallel\langle v_\perp^3 {J_0'}^2\rangle\chi,$$

$$\lambda_{23} = -i\sum_n\frac{\omega_p^2 k_\parallel}{\omega n^2\Omega^2}\left[\langle v_\perp^2 J_n J_n'\rangle + 2\langle v_\parallel^2\rangle\langle v_\perp J_n J_n'\frac{\partial}{\partial v_\perp}\rangle\right] - i\frac{\omega_p^2}{\omega}\langle v_\perp^2 J_0 J_0'\rangle\chi, \tag{A22}$$

$$\lambda_{33} = -\frac{\omega_p^2}{\omega^2}\left[1-\langle v_\parallel^2\rangle\langle J_0^2\frac{\partial}{\partial v_\perp}\rangle\right] + \frac{\omega_p^2}{\omega^2}\langle v_\perp J_0^2\rangle\left(1+\frac{\omega^2}{k_\parallel}\chi\right). \tag{A23}$$

The general dispersion relation is obtained from the determinant $\det|D| = 0$, where $D_{ij} = N^2\delta_{ij} - N_i N_j - \epsilon_{ij}$. Further simplifications are possible in the long wavelength limit.

Appendix B: long wavelength approximation

In this appendix we provide general expressions for the dielectric tensor in the long wavelength limit $k_\perp v_\perp/\Omega \ll 1$, where $J_{\pm 1} = \pm k_\perp v_\perp/2\Omega$, $J_0 = 1 - k_\perp^2 v_\perp^2/2\Omega^2$, and higher order Bessel functions may be neglected. In this limit one has

$$\lambda_{11} = \frac{\omega_p^2}{\Omega^2} + \tfrac{1}{2}N_\parallel^2(\beta_\parallel - \beta_\perp), \tag{B1}$$

$$\lambda_{12} = i\frac{\omega_p^2}{\omega\Omega}, \tag{B2}$$

$$\lambda_{13} = -\tfrac{1}{2}N_\parallel N_\perp(\beta_\parallel - \beta_\perp), \tag{B3}$$

$$\lambda_{22} = \frac{\omega_p^2}{\Omega^2} + \tfrac{1}{2}N_\parallel^2(\beta_\parallel - \beta_\perp) \tag{B4}$$

$$- N_\perp^2\beta_\perp + \frac{N_\perp^2\beta_\perp}{4}\frac{\langle v_\perp^4\rangle}{\langle v_\perp^2\rangle}\chi],$$

$$\lambda_{23} = i\frac{\beta_\perp \tan\theta\Omega}{2\omega}c^2\chi, \tag{B5}$$

$$\lambda_{33} = \tfrac{1}{2}N_\perp^2(\beta_\parallel - \beta_\perp) + (\frac{\omega_p^2}{k_\parallel^2} - \frac{\beta_\perp \tan^2\theta c^2}{2})\chi, \tag{B6}$$

where $N = kc/\omega$, $N_\perp = k_\perp c/\omega = N\sin\theta$, $N_\parallel = lk_\parallel c/\omega = N\cos\theta$, $\beta_\parallel = 2\omega_p^2\langle v_\parallel^2\rangle/c^2\Omega^2$, $\beta_\perp = \omega_p^2\langle v_\perp^2\rangle/c^2\Omega^2$, and $\langle\ldots\rangle$ denotes usual averaging over the distribution. Here also $\zeta = u - v_\parallel$, where $u = \omega/k_\parallel$. The last term in (B6) is given for completeness. In the limit used in this paper, $\omega/\Omega \to 0$ and ω/k finite, it should be neglected. Throughout the paper we also assume $\omega_{pi} \gg \Omega_i$.

Appendix C: Aperiodic nature of the mirror instability

In order to show that the mirror instability is aperiodic we analyze the behavior of the roots of (9) when the β parameters are changed. In the waterbag case the transition from the stable to the unstable regimes occurs when $W = 0, G = 0$ and for the mode whose phase velocity is less than the highest particle velocity, $\mathrm{Re}\, Z < v_{\parallel,\max}$ ("subparticle" mode), that is, in the resonant region. In the general case, where Landau damping is nonzero, in the resonant range every propagating wave having $W \neq 0$ has also nonzero damping rate $G < 0$ (we assume that there are no other kinetic instabilities in the mirror-stable region). By continuously changing the plasma parameters (e.g., the anisotropy ratio $\beta_\perp/\beta_\parallel$) we can bring the system into the unstable regime. Assuming continuous dependence of W and G on the plasma parameters we see that it is impossible for the "subparticle" mode with $W \neq 0$ to transform into the unstable mode, since $G < 0$ and cannot be made positive continuously. Thus, the only way to do that is to go through $W = 0, G = 0$.

Let us now consider the vicinity of the transition to the instability, $|Z| \ll 1$. In the most general way, expanding $\bar\chi$ in powers of Z one gets:

$$\begin{aligned}\bar\chi &= \int \frac{1}{Z - v_\parallel}\frac{\partial f}{\partial v_\parallel}dv_\parallel \\ &= -\int \frac{1}{v_\parallel}\frac{\partial f}{\partial v_\parallel}dv_\parallel + Z\int \frac{1}{Z - v_\parallel}\frac{1}{v_\parallel}\frac{\partial f}{\partial v_\parallel}dv_\parallel \\ &\to d + i\kappa Z,\end{aligned} \tag{C1}$$

provided $(\partial f/\partial v_\parallel)|_{v_\parallel=0} \neq 0$. The quantities d and κ are defined in (13). It is easy to see that (9) is the first order equation for iZ (with real coefficients) in the lowest order on $|Z| \ll 1$, which means that there is a simple (one and only one) aperiodic root in the vicinity of $Z = 0$. Such aperiodic solutions cannot be converted into non-aperiodic ones by continuous change of the plasma parameters, for the same reason as above. Therefore, the unstable solutions must be aperiodic.

The function $\Psi(Z)$, defined in (9), is an analytical function of $Z = W + iG$ and a continuous function of its parameters β and θ. Let us consider how Z moves from the lower half-plane (stable regime) to the upper half-plane (unstable regime) with the change of β and θ = const. The transition to instability occurs, in general, in the vicinity of $Z = 0$ where $\Psi(Z) = \Psi(0) + (d\Psi/dZ)|_{Z=0}Z = A + BZ$ (see sec. V). In the transition point $A = 0$. Using (14)–(16) it is easy to show that in the transition point $B > 0$ (provided $\kappa > 0$, this condition being violated if $\partial f/\partial\mathcal{E} > 0$ at $v_\parallel = 0$, corresponding to the regime of two-hump instability), so that in the vicinity of the transition point $A > 0$ corresponds to the stable regime, while $A < 0$ corresponds to the instability. Because of the continuity, in the whole instability range $A < 0$.

Let us show now that (9) always has a solution $Z = iG$, $G > 0$ in the unstable range. Indeed, $\Psi(0) < 0$ as is shown above. On the other hand, if $G \to \infty$ one has $\chi \to 1/G^2$ and $\Psi(\infty) > 0$. This means that there exists $G > 0$ such that $\Psi(G) = 0$.

In the absence of kinetic instabilities, in the stable regime all roots of (9) with nonzero W are either in the lower half-plane (Landau damping or nonpropagation) or at the real axis (if $(\partial f/\partial v_\parallel)|_{v_\parallel=W} = 0$). In the first case no root can cross the real axis except at $W = 0$, when the parameters are changed continuously to bring the system in the unstable regime. As can be seen from (14)–(16) there is only one root crossing the real axis at this point, provided $\partial f/\partial\mathcal{E} < 0$. Therefore, there is only one root in the upper half-plane and it is purely imaginary.

If $\partial f/\partial \mathcal{E} = 0$ there are two or more roots in the vicinity of $Z = 0$ (depending on the behavior of f) but only one is positive, $G > 0$. Since in this case the analytical continuation through $Z = 0$ into the lower half-plane is straightforward (no pole at $v_\parallel = 0$), other roots correspond to damping solutions, and there is again only one root in the upper half-plane.

Finally, let us consider the case where there are roots with $G = 0$ and $W = W_0 \neq 0$. Such a situation can occur when $(\partial f/\partial v_\parallel) = 0$ in isolated points or in an interval (as for the compact waterbag and hard-bell). In the first case the imaginary part of Z is negative for W close to W_0, so that the continuous change of parameters does not bring the root to the upper half-plane. In the second case the continuous change of parameters leaves the root on the real axis until it enters the range where $(\partial f/\partial v_\parallel) \neq 0$ or $W = 0$.

---

[1] D. Krauss-Varban, N. Omidi, K.B. Quest, J. Geophys. Res., 99, 5987 (1994).
[2] D. S. Orlowski, C. T. Russell, D. Krauss-Varban, N. Omidi, J. Geophys. Res., 99, 169 (1994).
[3] R.L. Kaufmann, J.T. Horng, A. Wolfe, A., J. Geophys. Res., 75, 4666 (1970).
[4] B.T. Tsurutani, E.J. Smith, R.R. Anderson, K.W. Ogilvie, J.D. Scudder, D.N. Baker, S.J. Bame, J. Geophys. Res., 87, 6060 (1982).
[5] L. Violante, B. Bavassano-Cattaneo, G. Moreno, J.D. Richardson, J. Geophys. Res., 100, 12047 (1995).
[6] A. Czaykowska, T.M. Bauer, R.A. Treumann, W. Baumjohann, J. Geophys. Res., 103, 4747 (1998).
[7] G. Chisham, S.J. Schwartz, M. Balikhin, M.W. Dunlop, J. Geophys. Res., 104, 437 (1999).
[8] M.A. Balikhin, S.J. Schwartz, S.N. Walker, H. Alleyne, M.W. Dunlop, Dual Spacecraft Observations of Standing Waves in the Magnetosheath, J. Geophys. Res.(in press).
[9] D. Winterhalter, M. Neugebauer, B.E. Goldstein, E.J. Smith, S.J. Bame, A. Balogh, J. Geophys. Res., 99, 23,371 (1994).
[10] C.T. Russell, W. Riedler, K. Schwingenschuch, Y. Yeroshenko, Geophys. Res. Lett., 14, 644 (1987).
[11] O.L. Vaisberg, C.T. Russell, J.G. Luhmann, K. Schwingenschuch, Geophys. Res. Lett., 16, 5 (1989).
[12] M.G. Kivelson, K.K. Khurana, R.J. Walker, J. Warnecke, C.T. Russell, J.A. Linker, D.J. Southwood, C. Polansky, Science, 274, 396 (1996).
[13] C.T. Russell, D.E. Huddleston, R.J. Strangeway, X. Blanco-Cano, M.G. Kivelson, K.K. Khurana, L.A. Frank, W. Paterson, D.A. Gurnett, W.S. Kurth, J. Geophys. Res., 104, 17,471 (1999).
[14] A. Hasegawa, A., Plasma instabilities and nonlinear effects (Springer-Verlag, New York, 1975).
[15] S.P. Gary, J. Geophys. Res., 97, 8519 (1992).
[16] M.E. McKean, D. Winske, S.P. Gary, J. Geophys. Res., 97, 19,421 (1992).
[17] S.P. Gary, S.A. Fuselier, B.J. Anderson, J. Geophys. Res., 98, 1481 (1993).
[18] D.J. Southwood, M.G. Kivelson, J. Geophys. Res., 98, 9181 (1993).
[19] F.G.E. Pantellini, S.J. Schwartz, J. Geophys. Res., 100, 3539 (1995).
[20] O.A. Pokhotelov, M.A. Balikhin, H.S.C.K. Alleyne, O.G. Onishchenko, J. Geophys. Res., 105, 2393 (2000).
[21] M.G. Kivelson, D.J. Southwood, J. Geophys. Res., 101, 17,365 (1996).
[22] N. Sckopke, G. Paschmann, A.L. Brinca, C.W. Carlson, H. Luhr, J. Geophys. Res., 95, 6337 (1990).
[23] D.J. Rose, Phys. Fluids, 8, 951, 1965.
[24] S. Ichimaru, Basic principles of plasma physics (W.A. Benjamin, Inc., Reading, Massachusetts, 1973).
[25] M. Abramowitz, I.A. Stegun, Handbook of mathematical functions (G.P.O. , Washington D.C., 1964).